Optical and Quantum Electronics **30** *(1998) 193–200*

Three-photon absorption in InAs

M. P. HASSELBECK*, A. A. SAID‡, E. W. VAN STRYLAND
Center for Research and Education in Optics and Lasers (CREOL), University of Central Florida, Orlando, FL 32816, USA

M. SHEIK-BAHAE
Department of Physics and Astronomy, University of New Mexico, Albuquerque, NM 87131, USA

Received 22 September 1997; revised and accepted 5 January 1998

Using 125 ps laser pulses, we observe three-photon absorption in room temperature InAs at a wavelength of 9.54 μm. This effect is readily identified by temperature-tuning the semiconductor bandgap through the three-photon absorption edge. A three-photon absorption coefficient of $K_3 = 1 \pm 0.6 \times 10^{-3}$ cm^3 MW^{-2} is extracted from non-linear absorption data obtained with an open-aperture Z-scan. Time-resolved measurement at high irradiance reveals an increase of absorption due to hot carriers. We also present an autocorrelation measurement of our CO_2 laser pulse that shows two complete optical free-induction-decay cycles.

1. Introduction

It is well known that two-photon absorption has implications for the operation of high-speed photonic devices. Only recently were limitations due to three-photon absorption (3PA) discovered [1, 2]. While two-photon absorption has been extensively studied in semiconductors, much less is known about 3PA. The former process has been identified in InAs in experiments by Elsaesser *et al.* [3] and Murdin *et al.* [4]. Kovalev and Surov [5] studied phase-conjugation of 10.6 μm laser pulses using room temperature InAs plates and attributed the non-linear polarization to 3PA. Unless the semiconductor is heated well above room temperature, however, the three-photon energy at 10.6 μm is insufficient to bridge the energy bandgap. Additionally, analysis of the experiment in [5] is difficult because the 100 ns timescale introduces uncertainty from recombination of photocarriers, while lack of axial mode control in their laser causes substantial shot-to-shot fluctuations. We avoid these problems in our experiment by using a shorter wavelength, much shorter pulses, and a reproducible, well-characterized laser beam.

2. Laser pulse characterization

Our measurements are made with an amplified TEA CO_2 laser and an optical free-induction-decay (OFID) pulse-slicing scheme [6–9]. This system has been described

*Present address: Max-Born-Institute for Nonlinear Optics and Ultrafast Spectroscopy, D-12489, Berlin, Germany; also with: USAF Philips Laboratory, KAFB, NM 87117.
‡Present address: Accuphotonics Inc., 2901 Hubbard Dr., Ann Arbor, MI 48105, USA.

0306-8919

extensively in the literature and only a brief outline is given here. Pulses from a single (transverse and axial) mode TEA laser are focused to obtain a gas-breakdown ($\sim 10^{11}$ W cm^{-2}) in a plasma-shutter [7]. The plasma, which occurs near the peak of the CO_2 laser pulse, is optically dense at the mid-infrared laser frequency and forms on a sub-nanosecond timescale. The truncated pulse enters a resonant absorber of heated, low pressure CO_2 gas [8]. If the plasma truncation time is comparable to or less than the dephasing time of the absorber gas, a short transient of laser light can propagate through the absorber experiencing very little attenuation. The duration of the transient is determined by the plasma-shutter speed and the free-induction-decay time of the absorbing molecules (T_2), which can be changed by adjusting the gas pressure [6]. CO_2 laser pulses as short as 20 ps have been produced by this technique [9].

In Fig. 1a, we present zero-background autocorrelation data of our OFID laser pulse at $\lambda = 10.6$ μm. A 3.3 cm length of thallium arsenic selenide is used to obtain signals at the second harmonic frequency [10]. Note the main lobe centred at zero delay and the pronounced wings. The central pulse and wings are caused by the first and second OFID decay pulses respectively, emitted by the 100 torr CO_2 absorber gas. We believe this is the first time the second pulse (i.e. ringing) in such a laser system has ever been observed. The dashed line is a fit to the data using the model of Sheik-Bahae and Kwok [9], with the plasma shutter speed the only free parameter. We deduce a shutter speed of 100 ± 5 ps, assuming a half-Gaussian truncation function to model the action of the plasma shutter. Much faster shutter speeds can be obtained with higher irradiance. Our fitting analysis shows that the central lobe of the autocorrelation data is determined almost entirely by the plasma formation time, while the wings are sensitive only to the absorber gas pressure. This is consistent with the physical picture of the pulse-shaping process [6]. The temporal power profile extracted from the autocorrelation data is shown in Fig. 1b. The second pulse contains 26% of the total energy.

Using the same non-linear crystal, a pulse autocorrelation is obtained at a laser wavelength of 9.54 μm (Fig. 1c). Because the crystal is cut for phase-matching at 10.6 μm, the second-harmonic signals are much weaker and only the primary pulse can be resolved. The nature of OFID pulse generation, however, leads to essentially identical beam behaviour at both wavelengths. The same fitting function used in Fig. 1a reasonably describes the shorter wavelength data in Fig. 1c (dashed line). The temporal profile depicted in Fig. 1b, along with carefully characterized Gaussian beam spatial-profiles are incorporated in our analysis of non-linear absorption in InAs discussed below.

3. Three-photon absorption experiments

Open aperture Z-scan measurements ($z_o = 1.35$ mm) of non-linear absorption are performed with an uncoated, 1 mm thick sample of bulk n-InAs mounted on the coldfinger of a closed-cycle helium cryostat [11]. Peak laser irradiance at the centre of the scan is ~ 70 MW cm^{-2}. The wafer is oriented at an angle of $\sim 30°$ from the optical axis (s-polarization) to eliminate etalon effects. A thin piece of indium wire serves as an interface between the sample and coldfinger. At a laser wavelength of 9.54 μm, three-photon transitions across the semiconductor bandgap are possible ($E_g = 0.36$ eV). Upon cooling to 15 K, however, the bandgap expands ($E_g = 0.42$ eV) to disable 3PA. This behaviour is clearly illustrated in the non-linear absorption data in Fig. 2, where only the sample temperature is changed in the two data sets.

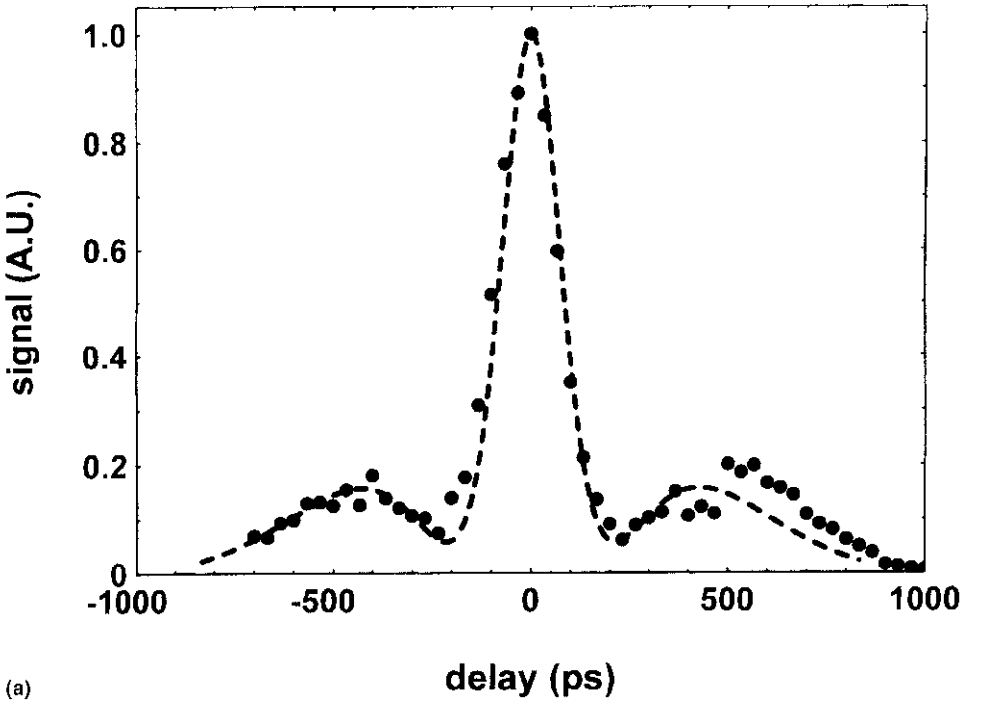

(a)

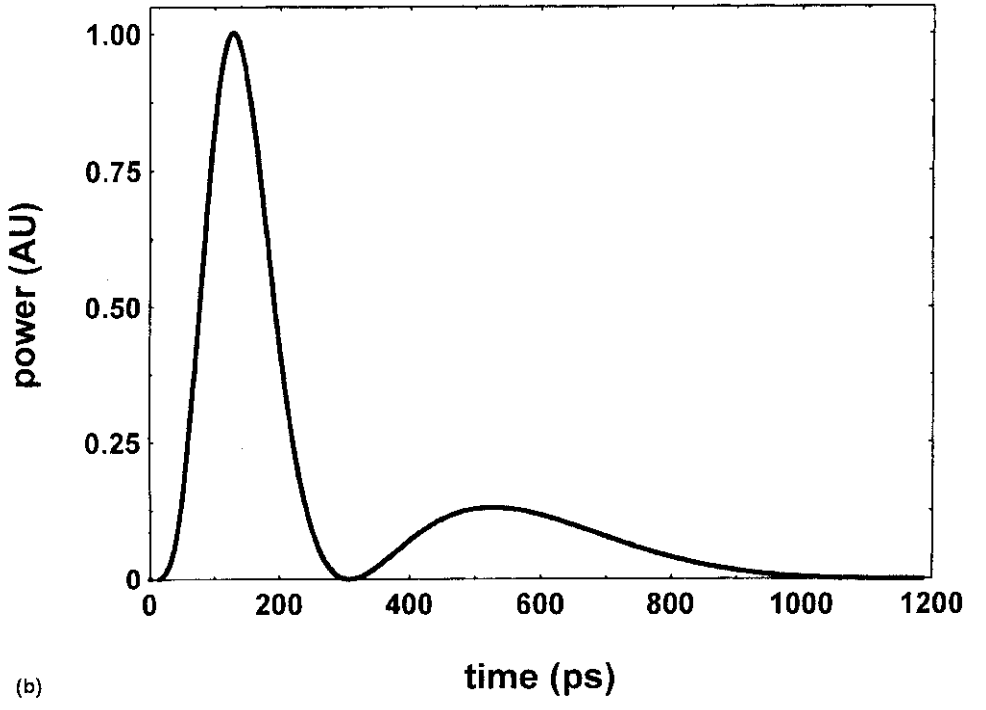

(b)

Figure 1 a, b

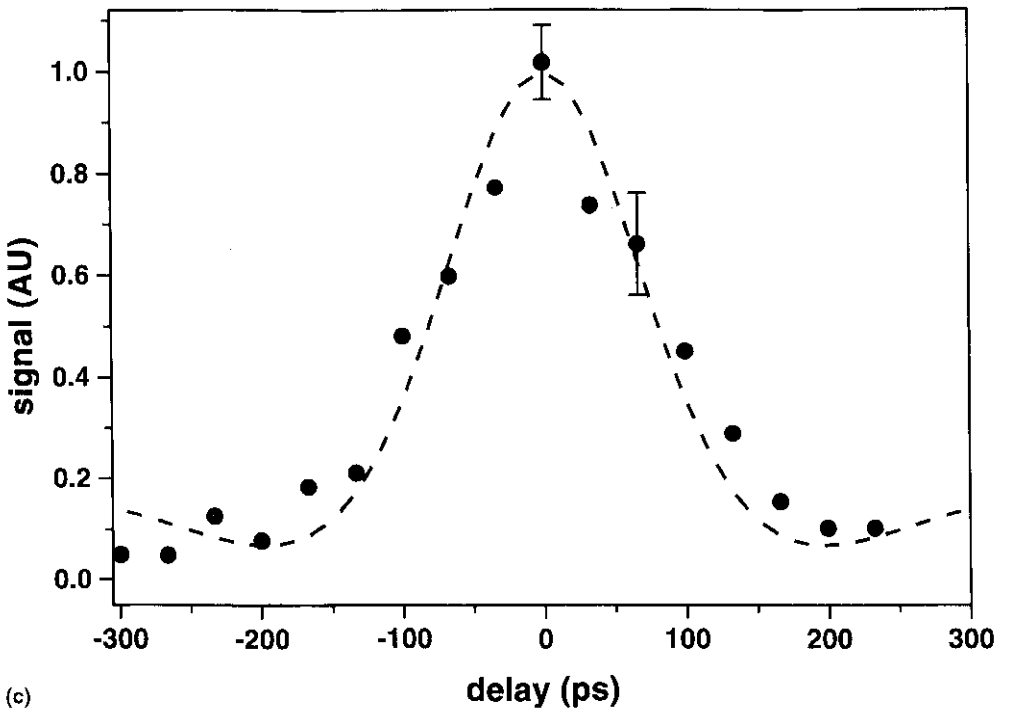

Figure 1 (a) Zero-background autocorrelation data of laser pulse at 10.6 μm (solid points). Dashed curve is a fit to the data using the model of [9]. (b) Deduced power profile of the laser pulse. (c) Autocorrelation data at 9.54 μm plot together with the curve used to fit the 10.6 μm data in (a).

The room temperature data are analysed with the usual model of non-linear propagation in a semiconductor in the presence of 3PA [1, 2]:

$$\frac{\partial}{\partial z} I(r,z,t) = -K_3 I^3 - (\sigma_e(I) N_e + \sigma_h(I) N_h) I \tag{1}$$

$$\frac{\partial}{\partial t} N_e(r,z,t) = \frac{\partial}{\partial t} N_h(r,z,t) = \frac{K_3 I^3}{3\hbar\omega} \tag{2}$$

where I is the temporally and spatially-varying laser irradiance, $\sigma_{e,h}$ are the electron and hole absorption cross-sections, N is the carrier density, and K_3 is the 3PA coefficient. Diffusion and recombination of carriers are ignored, the latter assumption justified by examination of the pump–probe data shown in Fig. 3.

The important absorption paths are depicted schematically in the E–k diagram in the inset of Fig. 2. Of the three different absorption components on the right-hand side of Equation 1, dipole-allowed transitions between the heavy and light-hole valence bands (corresponding to the path marked C and the term σ_H) are dominant [12, 13]. Intraband free carrier transitions require collisions with a third particle such as a phonon to conserve momentum and are approximately two orders of magnitude weaker than the intervalence

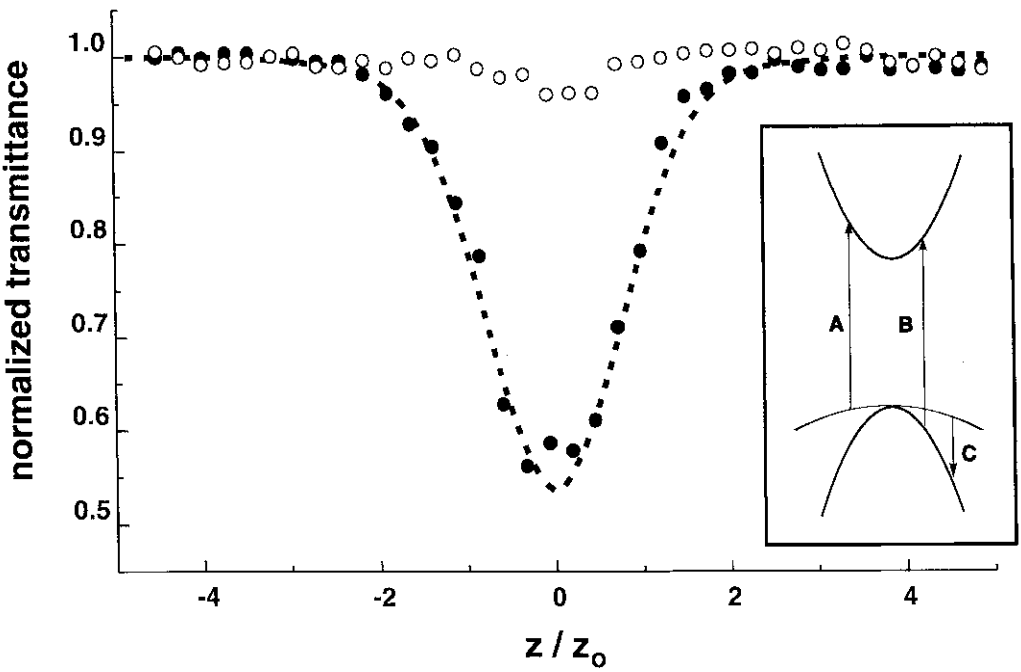

Figure 2 Open-aperture *Z*-scan data of InAs at room temperature (filled circles) and 15 K (open circles). Peak irradiance at the centre of both scans is ~70 MW cm^{-2}. The dashed line is obtained with a 3PA coefficient of $K_3 = 1 \times 10^{-3}$ cm^3 MW^{-2}. Inset: schematic of the relevant absorption paths: A, 3-photon absorption from the heavy-hole band; B, 3-photon absorption from the light-hole band; and C, single-photon linear absorption between the heavy- and light-hole bands.

band transition. Therefore we observe the linear absorption of heavy holes produced by 3PA. In order for direct 3PA (indicated by the heavy and light-hole bandgap transitions at A and B, respectively) to dominate the non-linear absorption, the irradiance must be significantly increased without a corresponding increase in energy, i.e. much shorter pulses are required.

Note that the free-carrier absorption cross-sections in Equation 1 are written as a function of irradiance. Figure 3a depicts the time-dependent differential absorption of heavy holes generated by 9.54 μm light at room temperature using the standard pump–probe arrangement. In this experiment, both beams are parallel polarized, but identical behaviour is obtained with perpendicular polarizations. The pump irradiance is ~200 MW cm^{-2}, or about a factor of 3 higher than the peak irradiance in the *Z*-scan measurement. The pump beam generates electron–hole pairs by 3PA. We find an enhanced absorption at short time delays, the decay of which is not resolved by our pulses. This is followed by a long-lived absorption signal due to photocarriers that recombine on a timescale longer than the measurement (> 1 ns). Similar behaviour is observed at a pump irradiance as low as ~120 MW cm^{-2}, which is near the detection limit of the weaker probe pulses. Because of tight focusing conditions, the overlap of pump and probe beams is uncertain preventing a detailed quantitative interpretation. We can, however, identify the

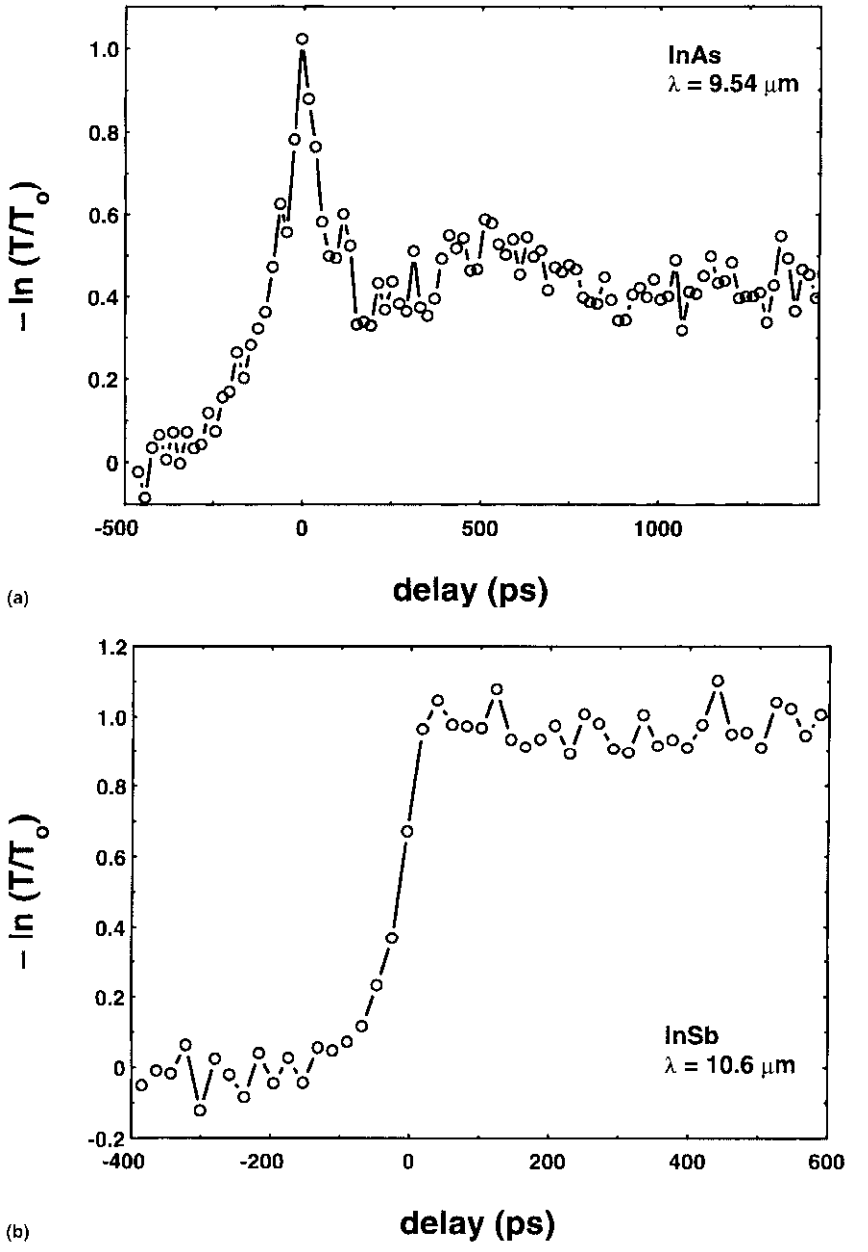

Figure 3 Time-resolved measurement of the heavy- to light-hole inter-valence band absorption (path C in Fig. 2) of room temperature semiconductor samples: (a) InAs at $\lambda = 9.54$ μm with pump irradiance approximately 200 MW cm ^{2}. The enhanced absorption at zero delay is caused by hot holes. (b) InSb at $\lambda = 10.6$ μm with pump irradiance approximately 50 MW cm^{-2}. Photocarriers are generated by two-photon absorption.

enhanced absorption signal at short time delays with the presence of hot carriers – specifically hot holes.

As a result of 3PA, a small amount of excess kinetic energy is given to the photocarriers ($\Delta E = 3\hbar\omega - E_g \cong 30$ meV). These carriers enter their respective distributions close to the bottom of the Γ-valley and thermalize to a temperature near the lattice temperature on a sub-picosecond timescale [14, 15]. The photogenerated holes reside almost entirely in the heavy-hole band [14]. Additional pump photons excite the thermalized holes from the heavy to light-hole band in regions of k-space well removed from the valley minimum. The light holes scatter rapidly (< 1 ps) to the heavy-hole band primarily by phonon emission mediated by the optical deformation potential, but with additional kinetic energy of the order of 100 meV. At sufficiently high pump irradiance, excitation to and scattering from the light-hole band heats the heavy-hole distribution. The high-energy tail of the hot heavy-hole distribution provides an additional population in the initial states of the inter-valence band transition and leads to the absorption spike in Fig. 3a. This is essentially the same dynamics observed by Woerner *et al.* [14, 16] in their experiments with p-type Ge. In polar semiconductors such as InAs, more irradiance is needed to generate comparable hole heating because of additional cooling provided by phonon emission via the polar optical mode [15]. When the pump pulse disappears, the photogenerated holes relax to the lattice temperature in ~30 ps [3]. This time is shorter than the resolution of our measurement, so the nearly constant absorption component at long delays in Fig. 3a is due to non-equilibrium holes at the lattice temperature that have not yet recombined.

Because of low signal levels, time-resolved absorption measurements were not possible at lower irradiance levels encountered in the InAs Z-scan experiment. To understand the behaviour of photocarriers in the irradiance regime of Fig. 2, a similar pump–probe measurement is made with room temperature InSb ($E_g = 0.18$ eV) at a longer wavelength of 10.6 μm (Fig. 3b). In this case, non-linear absorption is caused by two-photon transitions across the semiconductor bandgap ($\Delta E = 2\hbar\omega - E_g \cong 50$ meV) at excitation levels much lower than needed for InAs [17]. Gentler focusing can be used and probe photons are then readily detected. Analysis of the band structure of InAs and InSb shows that absorption takes place at similar regions of k-space in the two experiments. The multi-photon transitions occur at $k \cong 1 \times 10^6$ cm^{-1} for light-holes and $k \cong 1.4$–1.6×10^6 cm^{-1} for heavy-holes, while direct inter-valence band absorption of laser photons occurs at $k \cong 3 \times 10^6$ cm^{-1}. InSb can therefore provide an excellent representation of the photon-excited hole dynamics of InAs. At a pump irradiance of ~50 MW cm^{-2}, the time-resolved measurement in Fig. 3b shows no evidence of enhanced absorption due to hot carriers in InSb and we conclude that the same situation exists for InAs at a comparable irradiance. Therefore the irradiance-independent, linear hole absorption cross-section ($\sigma_H = 8 \times 10^{-16}$ cm^2) of InAs measured by Matossi and Stern [12] is appropriate for analysis of our Z-scan data.

The dashed curve in Fig. 2 is a fit to the data with a 3PA coefficient of $K_3 = 1 \pm 0.6 \times 10^{-3}$ cm^3 MW^{-2}, with the error range primarily associated with the uncertainty of the hole absorption cross-section. The deduced K_3 coefficient is in good agreement with Wherrett's model of 3PA employing third-order perturbation theory for allowed–allowed–allowed transitions between two parabolic bands [18] that yields $K_3 = 1.8 \times 10^{-3}$ cm^3 MW^{-2}. It should be pointed out that if the hole absorption did indeed increase appreciably in the high irradiance regime of Fig. 2 (centre of the Z-scan), the normalized transmittance of the sample would have been much lower. A factor of 2

increase of the free carrier absorption cross-section near the centre of the Z-scan, for example, would cause the data to trace out a significantly steeper valley suggesting even higher order non-linear behaviour. Our model of non-linear absorption with an irradiance-independent hole absorption cross-section reproduces the Z-scan data very well.

We comment on the absence of non-linear absorption in the Z-scan at 15 K. We have previously measured four-photon absorption in InAs at 10.6 μm and do not expect this to be important at a lattice temperature of 15 K with an irradiance less than 100 MW cm^{-2} [19]. Laser-induced impact ionization of electron hole pairs should not occur until the irradiance exceeds 300 MW cm^{-2}.

In summary, temperature-tuning the bandgap of InAs reveals a strong three-photon absorption resonance with 9.54 μm laser light. The deduced 3PA coefficient ($K_3 = 1 \pm 0.6 \times 10^{-3}$ cm^3 MW^{-2}) is consistent with Wherrett's theoretical formulation of multi-photon absorption for a two-band semiconductor. Analysis of the data can be complicated by the presence of hot holes, but we argue that in the relevant irradiance regime of our Z-scan measurement (< 75 MW cm^{-2}), this is of minor importance. We also presented autocorrelation data of 125 ps CO_2 laser pulses that shows two complete cycles of optical free-induction-decay. This data is well described by the model of [9] indicating a plasma shutter speed close to 100 ps.

Acknowledgements

We thank J. Patula for providing laboratory assistance. M. P. H. acknowledges the financial support of a Hughes Aircraft Company doctoral fellowship.

References

1. C. C. YANG, A. VILLENEUVE, G. STEGEMAN and J. S. AITCHISON, *Opt. Lett.* **17** (1992) 710.
2. J. KANG, A. VILLENEUVE, M. SHEIK-BAHAE, G. STEGEMAN, K. AL-HEMYARI, J. AITCHISON and C. IRONSIDE, *Appl. Phys. Lett.* **65** (1994) 147.
3. T. ELSAESSER, R. BÄUERLE and W. KAISER, *Infrared Phys.* **29** (1989) 503.
4. B. MURDIN, C. PIDGEON, A. KAR, D. JAROSZYNSKI, J.-M. ORTEGA, R. PRAZERES, F. GLOTIN and D. HUTCHINGS, *Opt. Mater.* **2** (1993) 89.
5. V. KOVALEV and M. SUROV, *Sov. J. Quantum. Electron.* **17** (1987) 386.
6. E. YABLONOVITCH and J. GOLDHAR, *Appl. Phys. Lett.* **25** (1974) 589.
7. H. S. KWOK and E. YABLONOVITCH, *Appl. Phys. Lett.* **27** (1975) 583.
8. H. S. KWOK and E. YABLONOVITCH, *Appl. Phys. Lett.* **30** (1977) 158.
9. M. SHEIK-BAHAE and H. S. KWOK, *Appl. Opt.* **24** (1985) 666.
10. D.R. SUHRE, *Appl. Phys. B* **52** (1991) 367.
11. M. SHEIK-BAHAE, A. A. SAID, T. H. WEI, D. J. HAGAN and E. W. VAN STRYLAND, *IEEE J. Quantum Electron.* **QE-26** (1990) 760.
12. F. MATOSSI and F. STERN, *Phys. Rev.* **111** (1958) 472.
13. R. CULPEPPER and J. DIXON, *J. Opt. Soc. Am.* **58** (1968) 96.
14. M. WOERNER, T. ELSAESSER and W. KAISER, *Phys. Rev. B* **45** (1992) 8378.
15. M. WOERNER and T. ELSAESSER, *Phys. Rev. B* **51** (1995) 17490.
16. M. WOERNER, T. ELSAESSER and W. KAISER, *Phys. Rev. B* **41** (1990) 5463.
17. M. SHEIK-BAHAE and H. S. KWOK, *IEEE J. Quantum Electron.* **QE-23** (1987) 1974.
18. B. S. WHERRETT, *J. Opt. Soc. Am B* **1** (1984) 67.
19. M. P. HASSELBECK, E. W. VAN STRYLAND and M. SHEIK-BAHAE, *J. Opt. Soc. Am. B* **14** (1997) 1616.